Full-field experimental and numerical characterisation of a growing fatigue crack in a stainless steel

S Alshammrei, B Lin, J Tong*

Mechanical Behaviour of Materials Laboratory, School of Mechanical and Design Engineering, University of Portsmouth, Anglesea Building, Anglesea Road, Portsmouth PO1 3DJ, UK

Abstract

Full-field mechanical characterisation has been carried out for growing cracks under cyclic loading conditions using both Digital Image Correlation (DIC) and integrated finite element (FE) analysis. Compact tension specimens of a model material, stainless steel 316L, were used in the experiments, where the position of the crack tip and the evolution of the near-tip displacements and strains were tracked at selected observation points along the crack path. "Critical" strains at the advancing crack tip were captured at selected locations along the crack path. The influence of DIC data processing strategies and the choice of a characteristic length on the critical strain were examined. Potential attenuation effects behind the crack tip, commonly referred to as crack closure, were also investigated by evaluating the crack opening displacement (COD) at selected instances to the crack tip during the crack growth, where the experiment was interrupted to allow DIC measurements taken during a complete cycle. The impact of measured crack closure on the near-tip strains and crack driving force in terms of J-integral was assessed using both standard and integrated FE analysis.

Keywords

Crack tip, DIC, fatigue crack growth, finite element, J-integral, strain

1. Introduction

Digital Image Correlation (DIC), as a Full-field measurement technique, has drastically improved our understanding of crack problems, when deformation and strain may be captured *in situ*, and the experimental data are then injected into finite element (FE) models so that more detailed analyses may be carried out under realistic boundary conditions. The basic principles of DIC for full-field displacement measurement were established in the 1980's, and the technique has been used for a range of engineering applications. Sutton and his associates [1] were the first to utilise DIC in the studies of fatigue and fracture mechanics, when crack opening displacements were obtained post fatigue testing and image acquisition. Crack growth resistance was studied in a functionally graded material [2], where a region of K-dominance was established. Fracture mechanics parameters, such as K and T, were identified from DIC analyses for essentially linear elastic cases [3]; whilst DIC mapping of displacement fields was used to obtain the J-integral [4,5]. Although a number of research have focused on crack problems, most early studies were carried out under monotonic or quasi-static loading conditions [1-5]. More recently, fatigue crack growth has been studied using DIC

* Corresponding author: jie.tong@port.ac.uk

[6-15] by mapping near-tip strains during fatigue crack growth at sub-grain level [8,9] and *in situ* [11-13, 15]. Specifically, Mathieu et al [7] developed image capture and post-processing strategies to determine the crack tip location, fracture mechanics parameters including K, T and plastic zone, as well as estimates of Paris law parameters. Carroll et al [8,9] used high resolution DIC and EBSD to capture accumulated plastic strain distributions at both macro and micro levels, and explored the relationship between plastic strain evolution and microstructure characteristics. Similarly, Ye et al [14] estimated von Mises strains and the plastic zone size at selected fatigue cycles.

Strain evolution with fatigue cycle has been captured, *in situ*, in stationery [11,12] and growing [12, 13, 15] crack cases by imaging at fixed observation points [11, 12] along the crack path [12, 13, 15]. The main purpose of our previous research aims at identifying a micromechanics crack driving force, based on the concept of strain ratchetting [16,17]. The fact that strain accumulates with cycle at a characteristic distance to the crack tip [11, 12] prompted research on growing cracks, where strains were captured *in situ*, so that a "critical" strain, or strain onset, may be identified when the crack tip approached an observation point. Although consistent results were obtained for the same material under similar loading conditions [12,13], significant variation in the measured critical strain data was obtained, prompting studies into the roles of post-processing parameters and the choice of the characteristic length. Furthermore, full-field tools such as DIC afford investigation of full crack tip field, both ahead and behind of the crack. Our most recent work on stationery cracks post fatigue pre-cracking seems to suggest that, whilst crack closure, as identified from COD, does occur during part of a loading/unloading cycle, it does not appear to impact on the near-tip strains ahead of the crack tip or the crack driving force [18,19]. It would be interesting to see if this is still true for the case of growing cracks, when the residual plastic strains left in the wake of an advancing crack are considered.

In this work, we report our most recent research on the concept of critical strain as a crack driving force for fatigue crack growth, examining some of the factors affecting the quantitative measure of this parameter using DIC. In addition, standard and integrated FE analyses were carried out to examine the impact of crack closure on the near-tip strains and the crack driving force in the case of a growing fatigue crack. We hope a more complete picture may emerge from the latest work to complement our previous research on stationery [11,12] and growing crack [12,13,15] work.

2. Experimental Procedures

2.1 Material and specimen geometry

The material used for this experiment is stainless steel 316L, which has a yield stress of 280 MPa, modulus of elasticity of 193 GPa and Poisson`s ratio of 0.3. An average grain size of the material was measured to be approximately 17µm. A compact tension specimen (CT) was employed with a thickness of 7 mm, width of 60 mm, and notch size of 12 mm. Prior to mechanical testing, speckle pattern was sprayed on the well-polished surface (mirror finish) of the metal for DIC analysis. Further experimental details are given elsewhere [12, 13].

2.2 Mechanical testing

Mechanical testing was carried out on an Instron servo-hydraulic testing machine (25kN). Pre-cracking was carried out under load-control using a load shedding scheme. The initial ΔK was 25 MPa$\sqrt{m}$, and the load was reduced manually step-by-step according to the measured crack length.

The load ratio and loading frequency were 0.1 and 10 Hz, respectively. Crack growth was monitored by surface replicas and direct current potential drop technique. The pre-cracking was terminated when the crack length reached a/W ≈ 0.30, $\Delta K \approx 15 MPa\sqrt{m}$. Mechanical testing was then carried out under cyclic load with $\Delta K = 25\ MPa\sqrt{m}$ (R=0.1) to allow steady-state fatigue crack growth at a rate approximately 10^{-7} m/cycle. Two series of experiments were carried out:

Series 1: Critical strain at the onset of crack growth

In order to investigate the development of strains ahead of the crack tip during fatigue crack growth the specimen was cyclically loaded from P_{min} to P_{max} at $\Delta K = 25\ MPa\sqrt{m}$, R=0.1. Periodically, the experiment was interrupted and DIC images were taken at the selected observation points at both minimum and maximum loads every 200 cycles. A total of 260 images were recorded during the fatigue crack growth from the initial crack length of 18.35 mm to the final crack length of 20.35 mm. A total of 13,000 cycles elapsed during the 2mm crack growth (Figure 2(a)).

Series 2: Crack Opening Displacement during fatigue crack growth

A CT Specimen was subjected to cyclic loading from P_{min} to P_{max} at $\Delta K = 25\ MPa\sqrt{m}$, R=0.1, and fatigue crack growth from an initial crack length of 19.40 mm to the final crack length of 19.71 mm was monitored during a crack growth of 310 µm in a total of 3000 cycles. The experiment was interrupted every 1000 cycles and 11 images were taken from minimum to maximum during a complete quasi-static cycle to measure CODs and near-tip strains.

2.3 Digital Image correlation

The imaging system (LAVISION GMBH) used for DIC analysis consisted of a CCD camera (2456 × 2058 pixels) and a Schneider Kreuznach F2.8 50 mm lens with 100 mm extension tubes. No filter was used in the data processing. A spatial resolution of 0.54 µm/pixel was achieved. A field of view (FOV), a rectangle of 1.2mm×1.1mm with the crack tip in the centre, was selected for imaging in order to capture the near-tip strain data ahead and COD data behind the crack tip. A subset size of 59x59 $pixels^2$ ≈ 30 x 30 µm and a step size of 14 pixels ≈ 7 µm were used to calculate the displacements and strains for the DIC analysis. Optical microscopy was also used to monitor the crack growth and to verify the crack tip position.

From Series 1 experiment, strain measurements were taken at the 20 observation points in an areas of interest (AOI) ahead of the crack tip along the perceived crack path, as shown in Figure 2 (a). The distance between each observation point is 100 µm. Normal strains were measured every 200 cycles, from which "critical" strains or instantaneous strains at the onset of crack growth were identified. The effects of the size of the measurement window (MW) on the measured strain values were examined. Selected sizes of MW were chosen to be 10x10, 20x20, 30x30, 50x50, and 100x100 μm^2, as shown in Figure 2(b).

For Series 2 experiment, COD was calculated from the displacement maps, where pairs of vertical displacements, at a fixed distance of 30 µm in the y-direction from the crack plane, were taken behind the crack tip at selected distances to the crack tip. The average vertical displacements at these positions were obtained and the CODs were obtained by subtracting the displacements on upper flank from those of lower flank, as illustrated in Figure 3. CODs were calculated at N=1000, 2000 and 3000 cycles at $\Delta K = 25\ MPa\sqrt{m}$ (R=0.1) and plots of COD vs P/P_{max} were produced.

3. Finite element analysis

3.1 The material model

Both kinematic and isotropic hardening were considered in the material stainless steel 316L (2.1) using a simple material model available in ABAQUS [21]. A total of five parameters in the constitutive model, including kinematic hardening parameters C and γ, initial yield stress σ_0 and isotropic hardening parameters Q_∞ and b, were determined from the cyclic experimental results for SS316L [22]. These material parameters, as well as Young's modulus E and Poisson's ratio υ, are presented in Table 1. The details of the material model were presented in ref [18].

3.2 Finite element analysis

A 2D FE model was developed for the geometry of the CT specimen used in the fatigue testing and DIC measurement, as described in Section 2. The FE analysis was carried out by using ABAQUS [21]. The FE model was meshed by 4-noded plane stress element (CPS4) with reduced integration and enhanced hourglass control to prevent both hourglass mode and shear locking during the analysis. A FE model mesh is shown in Figure 4(a), where refined element grids were applied around the perceived crack path. To register the grids between the FE model and the DIC consistently, the element size in the FOV (2.3) was selected to make the nodal spacing of the FE meshes matches the grid size of 7.74μm used in the DIC measurement, so that the potential errors were reduced when the DIC displacement fields were injected into the FE nodes as the boundary conditions for the integrated FE analysis. A mesh convergence analysis was carried out, and the results show that the crack tip deformation may be captured satisfactorily by a mesh size of 7.74 μm. To reduce the DIC image noise due to discontinuity of the crack, a region of DIC displacement data (0.65mm×0.1mm) around the crack was excluded [23], as shown in Figure 4(b). The effects of the size of the exclusion zone on the strains and J-integral were evaluated by using a different area without excluding any area ahead of the crack tip and by not excluding any data, and the differences in the results are found to be negligible.

No slip condition was assumed between the load pin the CT-specimen in the 2D FE model, and the cyclic loading was applied to the centre of the load pin. To simulate crack growth due to fatigue pre-cracking for the CT specimen, the crack-tip nodes were sequentially released, in which one node was released at the minimum applied loading after every two cycles to ensure that no abrupt change occurred in the open displacement [24]. Contact pairs were specified between the crack surfaces to prevent potential overlapping due to crack closure under fatigue loading. Both standard FE analysis and integrated FE analysis were carried out. The former used the applied load whilst the latter used the displacement data from the DIC [20] as the boundary conditions without loads. In the integrated FE analysis, the crack tip fields were updated at cycle N=1000, 2000 and 3000, using the DIC data recorded (2.2); and three FE models were created for the three cases reflective of the different crack lengths and displacement fields. The DIC displacement data recorded at N cycles were applied on the FE model as the boundary conditions to calculate the near-tip strains and CODs.

3.3 Modified J-integral in the presence of residual stresses

When plasticity-induced crack closure is present, residual stresses are produced on the crack flanks and the traction-free condition for standard J-integrals is violated. To obtain the path-independent J-integral in the presence of compressive residual stresses, initial strains were introduced into the standard J-integral equation so that the path-independency of J-integral may be restored. A modified J-integral equation is expressed as [25]:

$$J = \int_{\Gamma} (W\delta_{1i} - \sigma_{ij}\frac{\partial u_i}{\partial x_1})n_i ds + \int_A \sigma_{ij}\frac{\partial \varepsilon_{ij}^0}{\partial x_1} dA \quad (5)$$

where W is mechanical strain energy density; δ_{1i} is Kronecker's delta; u_i and σ_{ij} are components of displacement and stress, respectively; n_i is the unit vector normal to Γ, and ds is the path length along Γ; A is the area enclosed by Γ; x_1 is the coordinate in the local crack driving direction; ε_{ij}^0 is initial strain. In this equation, the first part, $\int_{\Gamma} (W\delta_{1i} - \sigma_{ij}\frac{\partial u_i}{\partial x_1})n_i ds$ is the standard J-integral expression, whilst the second part $\int_A \sigma_{ij}\frac{\partial \varepsilon_{ij}^0}{\partial x_1} dA$ is the new item introduced considering the initial strains on the J-integral, full details of the treatment is given elsewhere [19].

4. Results

4.1 Measurement of critical strain

The present study aims to examine the impact of the measurement strategy as well as the size of MW on the measured critical strain values. Selected sizes of MW were used to obtain the average normal strains at the incipient crack tip. Figure 5 shows the normal strains measured at the observation points (1-20, see Figure 2(a)) using a size of MW 10x10 μm^2. The average strain was calculated as 4.1%, whilst the standard deviation (SD) was estimated to be 1.16%. The effects of the size of MW on the critical strain as a function of number of cycles are shown in Figure 6(a); and the average strains measured as a function of MW is shown in Figure 6(b). It is clear that there are significant variations (SD=1.16%) in the measured strains during crack growth; and the variation is more evident when examined in detail (Figure 6(a)). The measured critical strain depends heavily on the size of MW, and high strain values are obtained using small MWs, as opposed to low strain values using large MWs. A "true" critical strain may be obtained from the extrapolation of normal strain vs size of MW curve (Figure 6(b)), which is estimated to be 5.24%.

4.2 Crack closure during fatigue crack growth

The phenomenon of crack closure was examined during the fatigue crack growth. The cyclic experiment was interrupted at three selected cycles, N=1000, 2000 and 3000, and CODs were measured at the selected locations behind the crack tip. The average crack growth during 1000 cycles is about 100μm, thus an average crack growth rate of 10^{-7}m/cycle. The deformation fields were injected into the FE model and integrated FE analyses were carried out. The CODs were then obtained from the FE analysis, both standard and integrated. Figure 7 shows the compliance curves measured by DIC and simulated by FE at the selected distances to crack tip (2Δ, 20Δ and 29Δ, Δ=17μm) at N=1000; 2000 and 3000 cycles. It seems that the results from DIC and FE are consistent in trend and quantitatively, and the measured "opening" varies with the distance to the crack tip, but also with time. Figure 8 shows the crack opening loads measured from the DIC and simulated from the integrated FE as a function of distance to the crack tip. Clearly the crack opening level registered is higher close to the crack tip (0.51-0.63) than those away from the crack tip (0.40-0.46). Close examination shows also greater sensitivity to time near the crack tip (0.51-0.63 at Δ), whilst

away from the crack tip (29Δ) the difference appears to diminish. This is possibly due to the greater accumulative effect of plastic deformation near the crack tip than that away from the crack tip.

4.3 Near-tip strains

The near-tip normal strains were examined using the integrated FE analysis (Figure 4), and the results at peak loads are presented in Figure 9 for a position close to the crack tip (2Δ) and one position away from the crack tip (10Δ) at the three instances: N=1000, 2000 and 3000 cycles. A comparison is made between the results from DIC, FE and HRR solution [26]. It seems that the DIC and FE results are similar in general, but they are significantly different from the HRR solution, particularly close to the crack tip. This is not entirely unexpected due to the high strain gradients and high noise levels close to the crack tip.

4.4 Crack driving force in the presence of crack closure

The impact of crack closure on the crack driving force J-integral during fatigue crack growth was examined in this work. Both standard and integrated FE analyses were carried out, from which the nominal and "effective" J-integrals were obtained, details of the procedure are given elsewhere [19]. The rationale is to assess if the J-integral is affected by crack closure, as identified in Figures 7 and 8, *during* fatigue crack growth. If so the J-integral from the integrated FE analysis should differ from that obtained by the standard FE analysis. Figure 10 shows the comparison of J-integrals from the standard FE (FE_{STD}) and the integrated FE (FE_{INT}) analysis at N=1000, 2000, 3000 cycles. It is clear that the results are essentially the same between the nominal and the "effective", and there seems no impact of crack closure on the crack driving force as represented by J-integral.

5. Discussion

One of the significant advantages of full-field studies of crack problems is to utilise the full-field information towards the identification of a physical crack driving force for fatigue crack growth. Towards this goal, we have proposed a concept of "critical strain" [16,17] from numerical studies of crack tip fields. This concept has since been tested using DIC in cases of stationery cracks [11,12] and growing cracks [12,13,15], and found it relevant to crack growth. Our previous work on SS316L [12,13] and a weld steel [15] has shown that it is possible to capture such a quantity using *in situ* monitoring of near-tip deformation fields in the presence of a growing fatigue crack. The essential approach is to assign a number of virtual observation points along the perceived crack path, from which DIC images are taken at regular intervals, *in situ*, during fatigue crack growth. The normal strains are then captured when the crack tip reached the observation point. It was found [12] that such strain values are highly sensitive to the size of the measurement window (MW), over which an average strain value was obtained as the critical strain. The effect of size of MW on the measured strain values was evaluated using three MWs (7.7μm×7.7μm; 15.4μm×15.4μm and 30.7μm×30.7μm). The results suggest that a small MW produces higher strain values as opposed to a large MW, due to the high strain gradient near the crack tip in the former; whilst the strain data are "smoothed" over a large MW in the latter. Nevertheless, a strain range of about 8% was found to be indicative of a critical value above which steady-state fatigue crack growth would occur in SS316L [13], consistent with the results from [12], despite of some differences between [13] and [12], including the DIC system/algorithm used, the spatial resolution and the load level.

In the present work, a more systematic evaluation has been carried out and results are presented in terms of critical strain vs the size of MW. This allows an extrapolation from which a "true" critical strain that independent of the size of measurement window may be obtained. Furthermore, the influence of crack wake on the critical strain has been examined in this work. As opposed to the position the crack tip placed in the centre of a MW at a given observation point, as in

[12,13], the present study positioned the crack tip on the edge of the MW, hence the average strain values are obtained from the displacement data ahead of the crack tip only. This has removed the DIC correlation errors behind the crack tip due to the discontinuity between the crack flanks. For this reason, the critical strain obtained in this work is notably lower than that reported in [12,13], although the quality of the present data has improved due to the exclusion of data behind the crack tip. Artificially high strain values are always obtained once the crack passes an observation point, as shown in Figure 5.

In our previous work [18,19], we challenged the concept of crack closure as an attenuation mechanism for fatigue crack growth. We investigated the issue by tracking the near-tip displacement fields of fatigue precracked specimens during loading and unloading, demonstrated the lack of attenuation effects on near-tip normal strain or J-integral in the presence of crack closure in the case of stationery cracks. A question was raised if the conclusion is still valid for a growing fatigue crack? To answer this question, we interrupted a growing fatigue crack periodically, and measured the deformation field each time. CODs were measured using both DIC and FE (Figures 7, 8); whilst near-tip normal strains (Figure 9) and J-integrals (Figure 10) were obtained using standard and integrated FE analysis. The results clearly confirm our hypothesis that, consistent with our previous work [19], there is no impact of crack closure on the crack driving force as represented by J-integral. Although our method of evaluating J considered only the loading part, a cyclic ΔJ was considered valid in the presence of crack closure [27].

6. Conclusions

Full-field characterisation of near-tip deformation has been carried out for growing cracks under cyclic loading conditions. The results from both Digital Image Correlation and integrated finite element analysis show that: i) A critical strain may be determined at a characteristic length to the crack tip by extrapolation to remove the impact of the size of measurement window and exclusion of the DIC data behind the crack tip. ii) Crack closure seems to be present during stable fatigue crack growth from COD measurements, although it does not appear to impact on the near-tip strains and the crack driving force in terms of J-integral.

Acknowledgements

Mr C Lupton for his assistance in the setting up of the experiments.

References

[1] M.A. Sutton, J.J. Orteu, H. Schreier, Image correlation for shape, motion and deformation measurements: Basic concepts, theory and applications, 1st ed., Springer US, Boston, MA, 2009. doi:10.1007/978-0-387-78747-3.

[2] J. Abanto-Bueno, J. Lambros, Investigation of crack growth in functionally graded materials using digital image correlation, Eng. Fract. Mech. 69 (2002) 1695–1711. doi:10.1016/S0013-7944(02)00058-9.

[3] S. Roux, J. Réthoré, F. Hild, Digital image correlation and fracture: an advanced technique for estimating stress intensity factors of 2D and 3D cracks, J. Phys. D. Appl. Phys. 42 (2009) 214004. doi:10.1088/0022-3727/42/21/214004.

[4] T.H. Becker, M. Mostafavi, R.B. Tait, T.J. Marrow, An approach to calculate the J-integral by digital image correlation displacement field measurement, Fatigue Fract. Eng. Mater. Struct. 35 (2012) 971–984. doi:10.1111/j.1460-2695.2012.01685.x.

[5] S.M. Barhli, M. Mostafavi, A.F. Cinar, D. Hollis, T.J. Marrow, J-Integral Calculation by Finite Element Processing of Measured Full-Field Surface Displacements, Exp. Mech. (2017). doi:10.1007/s11340-017-0275-1.

[6] S. Vanlanduit, J. Vanherzeele, R. Longo, P. Guillaume, A digital image correlation method for fatigue test experiments, Opt. Lasers Eng. 47 (2009) 371–378. doi:10.1016/j.optlaseng.2008.03.016.

[7] F. Mathieu, F. Hild, S. Roux, Identification of a crack propagation law by digital image correlation, Int. J. Fatigue. 36 (2012) 146–154. doi:10.1016/j.ijfatigue.2011.08.004.

[8] J.D. Carroll, W. Abuzaid, J. Lambros, H. Sehitoglu, High resolution digital image correlation measurements of strain accumulation in fatigue crack growth, Int. J. Fatigue. 57 (2013) 140–150. doi:10.1016/j.ijfatigue.2012.06.010.

[9] J.D. Carroll, W.Z. Abuzaid, J. Lambros, H. Sehitoglu, On the interactions between strain accumulation, microstructure, and fatigue crack behavior, Int. J. Fract. 180 (2013) 223–241. doi:10.1007/s10704-013-9813-8.

[10] P. Lopez-Crespo, B. Moreno, A. Lopez-Moreno, J. Zapatero, Characterisation of crack-tip fields in biaxial fatigue based on high-magnification image correlation and electro-spray technique, Int. J. Fatigue. 71 (2015) 17–25. doi:10.1016/j.ijfatigue.2014.02.016.

[11] J. Tong, B. Lin, Y.W. Lu, K. Madi, Y.H. Tai, J.R. Yates, V. Doquet, Near-tip strain evolution under cyclic loading: In situ experimental observation and numerical modelling, Int. J. Fatigue. 71 (2015) 45–52. doi:10.1016/j.ijfatigue.2014.02.013.

[12] Y.-W. Lu, C. Lupton, M.-L. Zhu, J. Tong, In Situ Experimental Study of Near-Tip Strain Evolution of Fatigue Cracks, Exp. Mech. 55 (2015) 1175–1185. doi:10.1007/s11340-015-0014-4.

[13] M.L. Zhu, Y.W. Lu, C. Lupton, J. Tong, In situ near-tip normal strain evolution of a growing fatigue crack, Fatigue Fract. Eng. Mater. Struct. (2016) 1–6. doi:10.1111/ffe.12391.

[14] S. Ye, J.-G. Gong, S.-T. Tu, X.-C. Zhang, C.-C. Zhang, Local strain accumulation in fatigue crack propagation process of Ti-6Al-4V alloy, Fatigue Fract. Eng. Mater. Struct. 40 (2017) 836–849. doi:10.1111/ffe.12559.

[15] T. Wigger, C. Lupton, S. Alshammrei, J. Tong, T.J. Marrow, P. Earp, M.-L. Zhu, D.-Q. Wang, T. Connolley, In situ mapping of normal strains in the field of a growing fatigue crack in a steel weld using digital image correlation and energy dispersive synchrotron X-ray diffraction, Int J Fatigue, 115 (2018) 11-19.

[16] L.G. Zhao, J. Tong, A viscoplastic study of crack-tip deformation and crack growth in a nickel-based superalloy at elevated temperature, J. Mech. Phys. Solids. 56 (2008) 3363–3378. doi:10.1016/j.jmps.2008.09.006.

[17] C. Cornet, L.G. Zhao, J. Tong, Ratchetting strain as a damage parameter in controlling crack growth at elevated temperature, Eng. Fract. Mech. 76 (2009) 2538–2553. doi:10.1016/j.engfracmech.2009.09.005.

[18] J. Tong, S. Alshammrei, T. Wigger, C. Lupton, J.R. Yates, Full-field characterization of a fatigue crack: Crack closure revisited. Fatigue Fract Eng Mater Struct. 141 (2018) 2130-2139.

[19] J. Tong, S. Alshammrei, B. Lin, T. Wigger, J Marrow, Fatigue Crack Closure: A Myth or A Misconception? Fatigue Fract Eng Mater Struct., in press.

[20] B. Lin, S. Alshammrei, T. Wigger, J. Tong, Characterisation of fatigue crack tip field in the presence of significant plasticity, Theoretical and Applied Fracture Mechanics, in press.

[21] ABAQUS 6.14, Hibbitt Karlsson and Sorensen Inc., Providence, RI, 2014.

[22] van Eeten p, Nilsson F. Constant and variable amplitude cyclic plasticity in 316L stainless steel. J Test Eval 2006; 34:298–311.

[23] Barhli SM, Mostafavi M, Cinar AF, Hollis D, Marrow TJ. J-integral calculation by finite element processing of measured full-field surface displacements. Exp Mech 2017; 57:997–1009.

[24] de Matos PFP, Nowell D. On the accurate assessment of crack opening and closing stresses in plasticity-induced fatigue crack closure problems. Eng Fract Mech 2007; 74:1579–1601.

[25] Lei Y, O'Dowd NP. Fracture mechanics analysis of a crack in a residual stress field. Int J Fract. 2000;106(3):195-216.

[26] Hutchinson JW. Singular behaviour at the end of a tensile crack in a hardening material. J Mech Phys Solids 1968;16:13-31.

[27] M. Metzger, T. Seifert, C. Schweizer. Does the cyclic J-integral ΔJ describe the crack-tip opening displacement in the presence of crack closure? Eng Fract Mech 2015; 134:459-473.

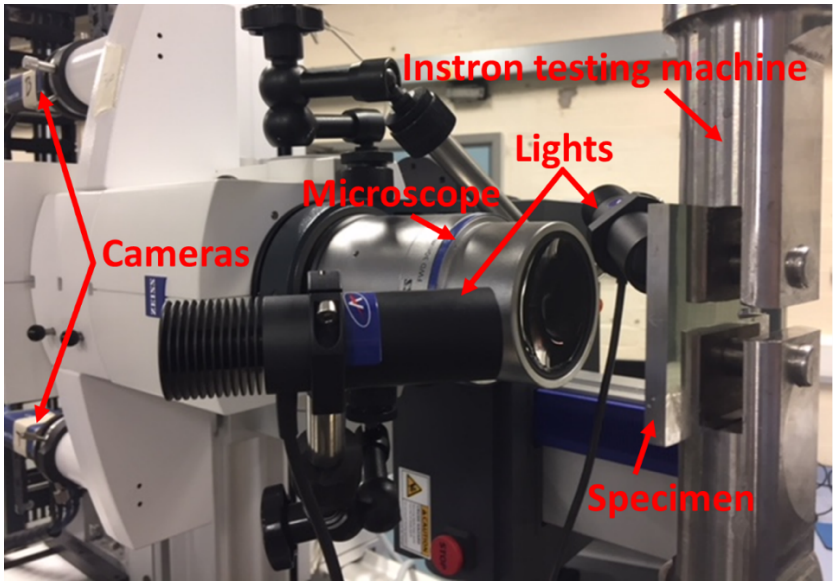

Figure 1. The experimental setup for fatigue testing and DIC imaging.

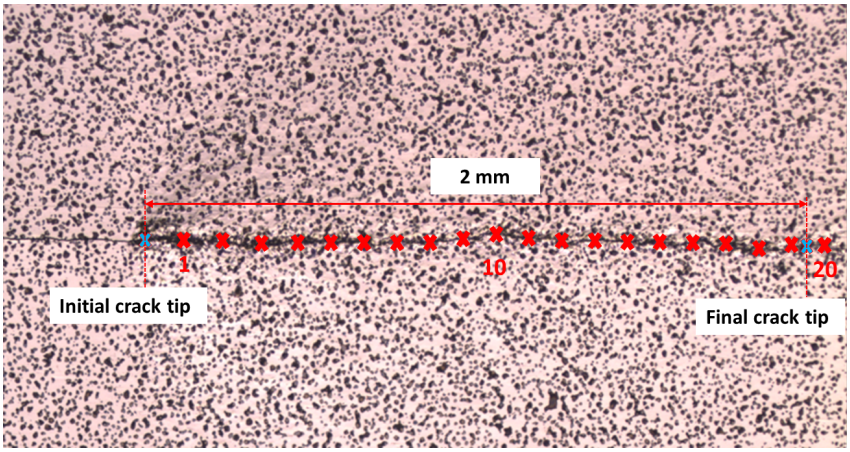

(a)

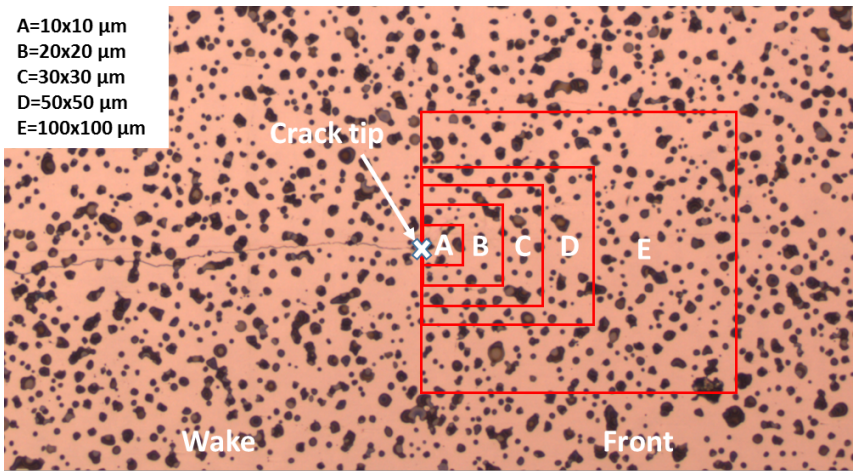

(b)

Figure 2. (a) The crack path and the observation points (red crosses) during the fatigue crack growth. The initial and the final crack tip positions are marked with blue crosses. (b) The selected sizes of measurement window (MW) used in the study.

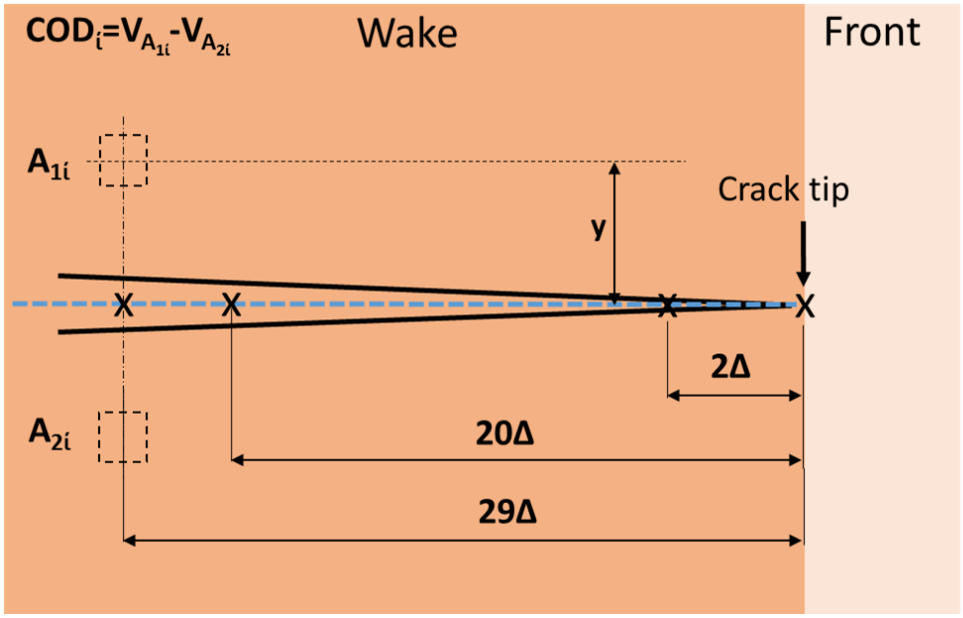

Figure 3. An illustration of the tracking points used for recording the CODs in the crack wake. The CODs were calculated from the vertical displacements of A1í and A2í at a fixed distance to the crack plane y (30 µm); whilst the tracking points were chosen to be multiples of the average grain size (Δ=17 µm) (jΔ, j =2, 20, 29).

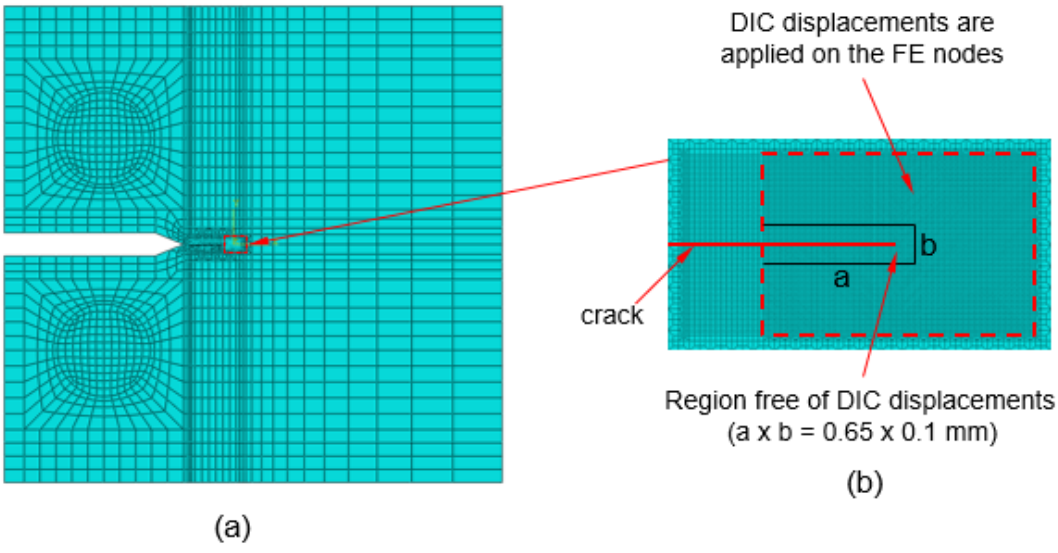

Figure 4. (a) The finite element model of the CT specimen used for the analysis; (b) the boundary conditions extracted from the displacements of FOV in the DIC analysis. A region of DIC data was excluded to reduce the measurement errors due to the presence of a crack.

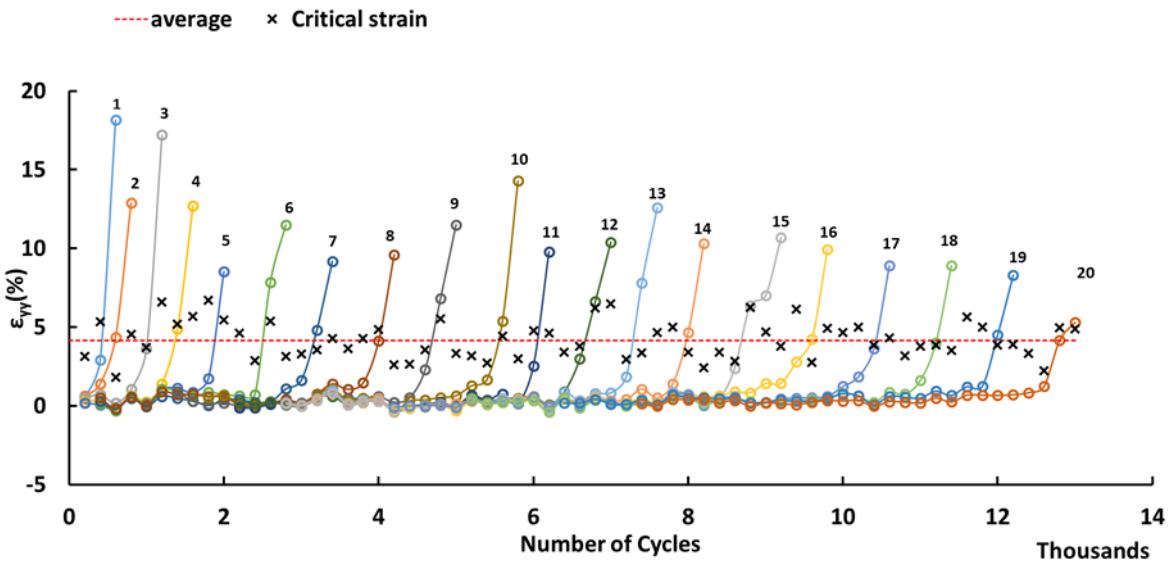

Figure 5. The normal strains measured at the observation points (Figure 2(a)) ahead of the crack tip. Symbol "x" represents the "critical" or onset strain when the crack tip reached the specific observation point (MW = 10 x10 μm²; SD =1.16 %).

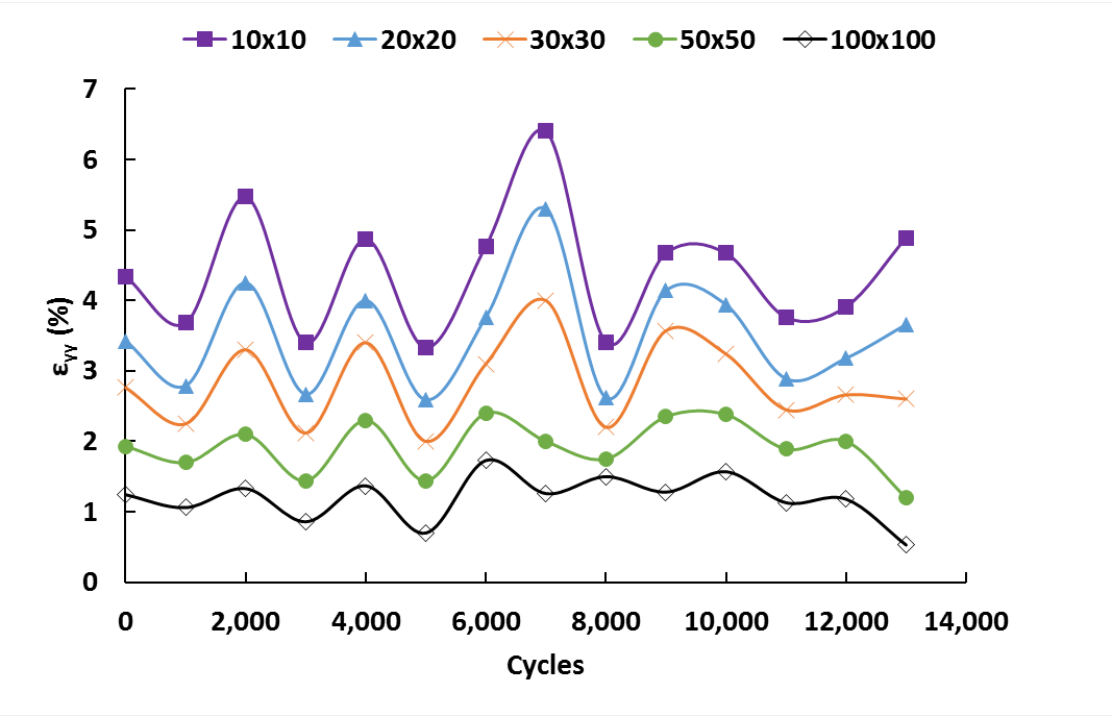

(a)

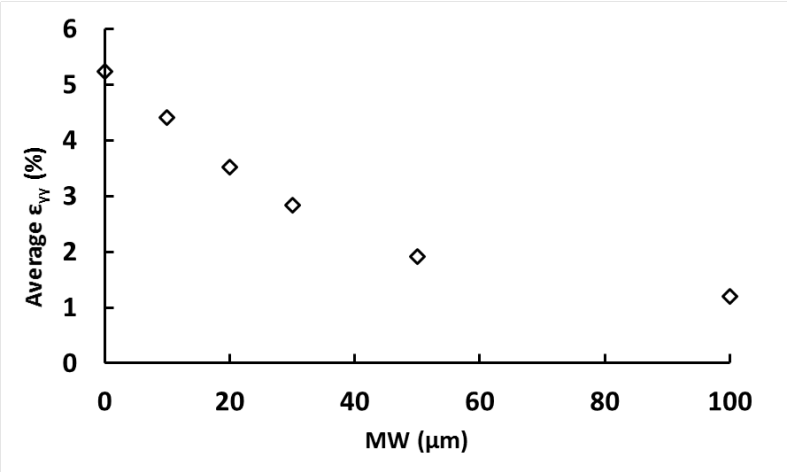

(b)

Figure 6. (a) The effects of the size of MW on the measured critical strain as a function of number of cycles. (b) The average critical strains measured as a function of the size of MW.

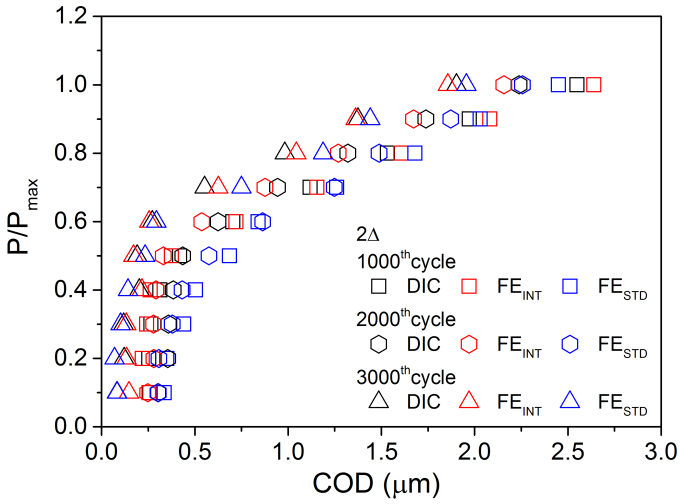
1.2
1.0
0.8
0.6
0.4
0.2
0.0
P/P max
0.0
0.5
1.0
1.5
2.0
2.5
3.0
COD (μm)
2Δ
1000th cycle
DIC
FE INT
FE STD
2000th cycle
DIC
FE INT
FE STD
3000th cycle
DIC
FE INT
FE STD

(a)

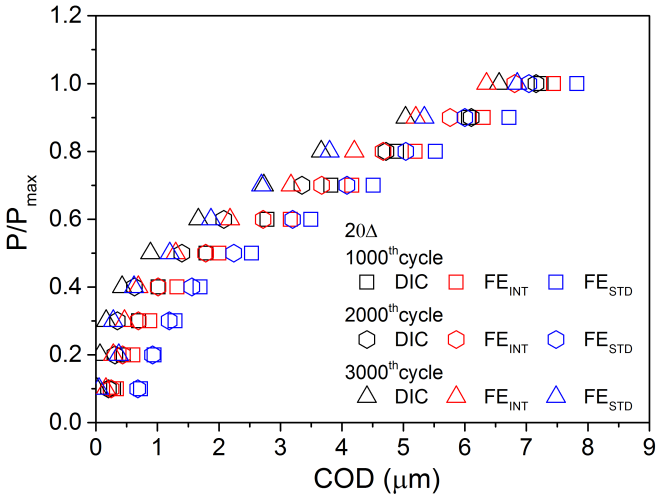
1.2
1.0
0.8
0.6
0.4
0.2
0.0
P/P max
0
1
2
3
4
5
6
7
8
9
COD (μm)
20Δ
1000th cycle
DIC
FE INT
FE STD
2000th cycle
DIC
FE INT
FE STD
3000th cycle
DIC
FE INT
FE STD

(b)

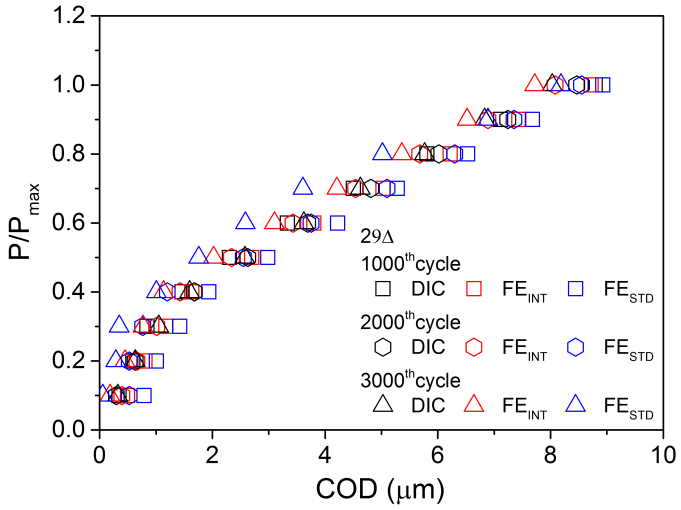

(c)

Figure 7. The compliance curves from DIC, integrated FE (FE_{INT}) and standard FE (FE_{STD}) at selected distances to crack tip a) 2Δ; b) 20Δ and c) 29Δ (Δ=17μm) at N=1000, 2000, 3000 cycles.

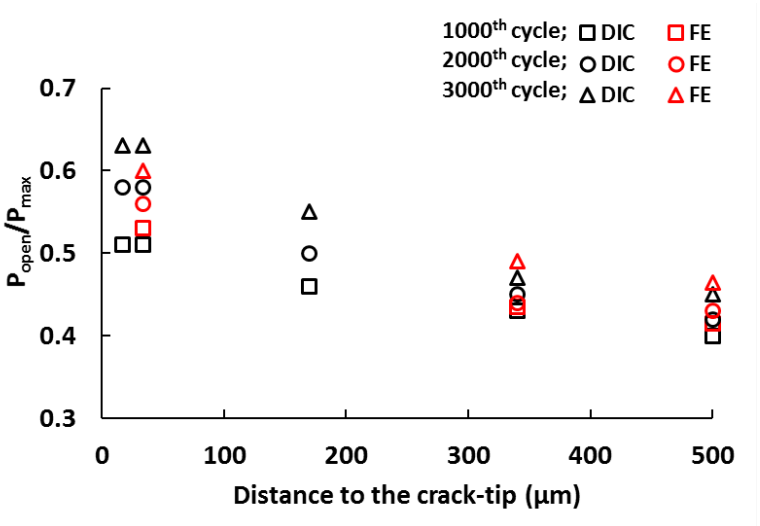

Figure 8. The crack opening loads measured from DIC and simulated from integrated FE as a function of distance to the crack tip at the selected number of cycles.

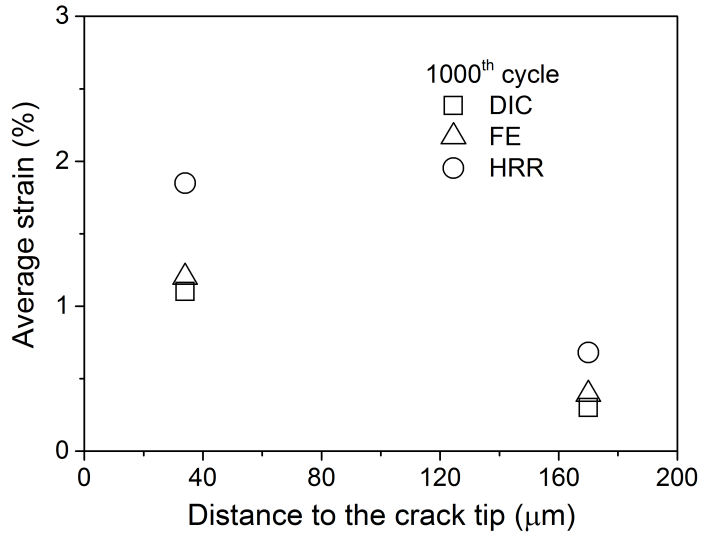
1000th cycle
DIC
FE
HRR
Average strain (%)
Distance to the crack tip (μm)
0
1
2
3
0
40
80
120
160
200

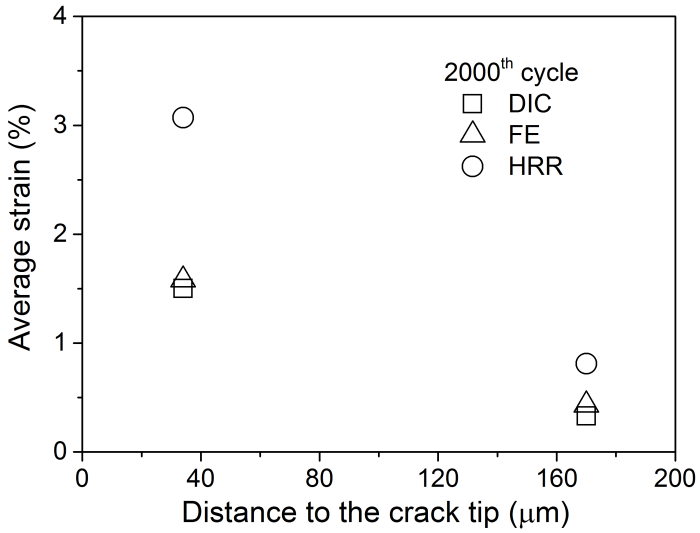
2000th cycle
DIC
FE
HRR
Average strain (%)
Distance to the crack tip (μm)
0
1
2
3
4
0
40
80
120
160
200

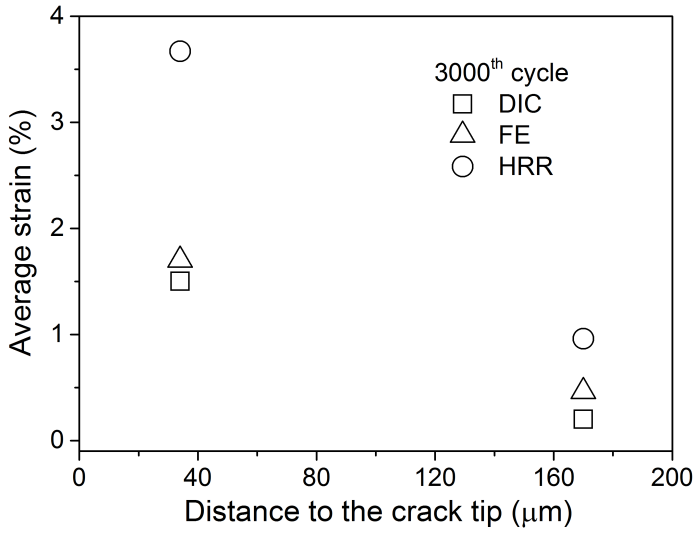

Figure 9. The average strains obtained from DIC, and FE analysis and the HRR solutions at N=1000, 2000, 3000 cycles.

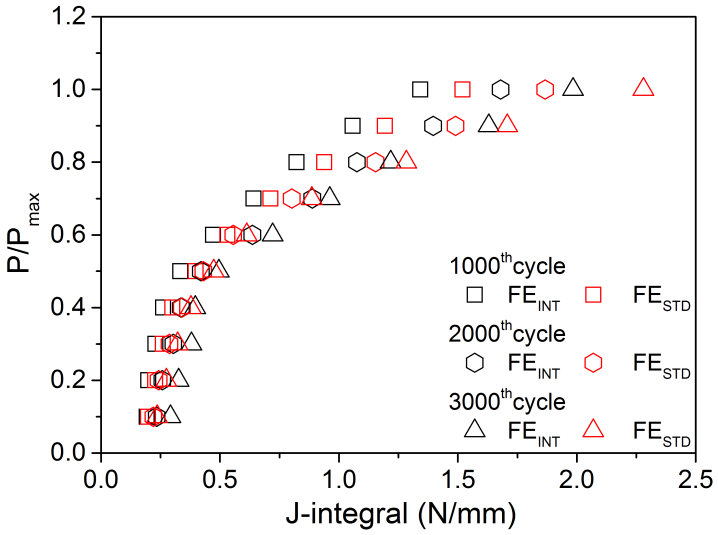

Figure 10. The J-integrals from the standard FE (FE_{STD}) and the integrated FE (FE_{INT}) analysis at N=1000, 2000, 3000 cycles.

Table 1. The material parameters for SS316L [18] used in the FE models

$E(GPa)$	υ	$\Delta\varepsilon(\%)$	$\sigma_0(MPa)$	Kinematic hardening		Isotropic hardening	
				$C(MPa)$	γ	$Q\infty$ (MPa)	b
193	0.3	4.0	100	60000	280	200	6